Nitroxide Complexes of Diruthenium(II,II) Carboxylates. Structural and Magnetic Properties

André Cogne,† Elie Belorizky,§ Jean Laugier,‡ and Paul Rey*,†

Commissariat à l'Energie Atomique, Laboratoire de Chimie de Coordination (URA CNRS 1194), Service d'Etudes des Systèmes et Architectures Moléculaires, Service de Physique des Matériaux et Microstructures, Département de Recherche Fondamentale sur la Matiére Condensée, Centre d'Etudes Nucléaires, BP 85X, 38041 Grenoble, France, and Laboratoire de Spectrométrie Physique (associé au CNRS), Université Joseph Fourier, BP 87, 38402 Saint Martin d'Hères Cedex, France

Received December 8, 1993®

The bis adduct of Tempo (2,2,6,6-tetramethylpiperidine-*N*-oxyl) with diruthenium (II,II) tetrakis(trifluoroacetate) has been prepared and characterized by x-ray diffraction at room and low (201 K) temperatures. It is a centrosymmetric complex in which the free radical ligands are axially bound. Its magnetic properties were studied in the 5–300 K temperature range and compared to those of the bis-THF dimetal precursor and to those of the diruthenium(II,II) tetrakis(perfluorobenzoate) bis-Tempo derivative. These properties were interpreted considering a large zero-field splitting within the dimetal core and nitroxyl–nitroxyl and diruthenium–nitroxyl exchange interactions. In the two bis-Tempo adducts the exchange interaction between the free radical and the dimetal center is antiferromagnetic and large ($\approx$300 cm^{-1}). It was not possible to assess the presence of internitroxyl coupling through the metal–metal double bond. Relevant crystallographic parameters at room temperature are as follows: triclinic system, space group $P\bar{1}$, a = 8.779(2) Å, b = 10.728(3) Å, c = 11.597(3) Å, α = 107.1(1)°, β = 103.3(1)°, γ = 107.2(1)°, Z = 2.

Investigations into the chemistry of nitroxide complexes of second row transition metals have, until now, been narrowly focussed. This is surprising in view of the interesting and highly diversified properties that first row and particularly copper(II) derivatives of these ligands are known to exhibit.[1-4] One factor in explaining this difference is the lack of appropriate metal precursors containing electron-withdrawing groups which would induce the binding of such weak Lewis bases as nitroxides. Only recently, dinuclear perfluorocarboxylates have been reported[5-7] for which solution studies had shown effective coordination of the nitroxide ligand.[8,9] Then, a few nitroxide derivatives involving the dirhodium core was characterized in the solid state.[10-12]

These μ-tetracarboxylato binuclear systems are attractive for two reasons. First, the nature of the carboxylate ligands is such that they offer minimal steric hindrance and bulky axial ligands can be accommodated without crowding complications; second, these metal–metal-bound species offer unprecedented through-bond pathways for mediating exchange interactions.[11,12] Following a thorough study of dirhodium derivatives, we report here a study of the Tempo (2,2,6,6-tetramethylpiperidine-1-oxyl) adducts with diruthenium(II,II) tetrakis(trifluoroacetate), $Ru_2(tfac)_4$, and diruthenium(II,II) tetrakis(perfluorobenzoate), $Ru_2(pfbz)_4$.

The dirhodium(II,II) frame corresponds to the $\sigma^2\pi^4\delta^2\delta^{*2}\pi^{*4}$ configuration[13] and, therefore, is diamagnetic. Magnetostructural correlations established from several nitroxide derivatives have proven unambiguously that exchange interactions are efficiently mediated by the singly bonded dimetal fragment and have suggested an important contribution of the σ orbitals to this process.[12] In contrast, the diruthenium analogue is paramagnetic and the metal atoms doubly bonded.[6] Although the nature of the ground state configuration has been disputed, evidences for a $\sigma^2\pi^4\delta^2\delta^{*2}\pi^{*2}$ configuration, which agrees with structural features and a triplet ground spin state, have been reported.[14] In preparing nitroxide derivatives of diruthenium carboxylates, we were primarily interested in obtaining extended species using nitronyl nitroxides as bridging ligands. In a first step however, the Tempo derivatives afford discrete offering the opportunity to get insight into possible coupling mechanisms in simple systems.

Since the temperature dependence of the magnetic susceptibility data of $Ru_2(tfac)_4(Tempo)_2$ exhibits a discontinuity at 243 K, both low (201 K) and room temperature structures have been determined. The structural features of this diruthenium nitroxide adduct are compared to the tetrahydrofuran precursor[6] and the dirhodium analogue;[11] the magnetic properties are compared to the closely related complex $Ru_2(pfbz)_4(Tempo)_2$.

Experimental Section

Syntheses. Tempo, $Ru_2(tfac)_4(THF)_2$ and $Ru_2(pfbz)_4(THF)_2$ were prepared following previously reported procedures.[6]

Syntheses of $Ru_2(tfac)_4(Tempo)_2$, 1, and $Ru_2(pfbz)_4(Tempo)_2$, 2. To a solution of 0.2 mmol of the appropriate diruthenium tetracarboxylate in 30 mL of dry benzene was added a solution of 0.4 mmol of Tempo in 10 mL of the same solvent. Precipitation of dark brown crystals immediately occurred. These were filtered and vacuum dried. **1**: 53%; mp 194 °C. Anal. Calcd for $C_{26}H_{36}F_{12}N_2O_{10}Ru_2$: C, 32.29; H, 3.75; F, 23.59; N, 2.90; O, 16.55; Ru, 20.92. Found: C, 31.98; H, 3.81; F, 24.01; N, 2.85; Ru, 21.12. **2**: 43%; mp 167 °C. Anal. Calcd for

† Laboratoire de Chimie de Coordination, Centre d'Etudes Nucléaires.
‡ Département de Recherche Fondamentale sur la Matiére Condensée, Centre d'Etudes Nucléaires.
§ Université Joseph Fourier.

® Abstract published in *Advance ACS Abstracts*, June 15, 1994.

(1) Eaton, S. S.; Eaton, G. R. *Coord. Chem. Rev.* **1978**, *26*, 207; **1988**, *83*, 29.
(2) *Magnetic Molecular Materials*, Gatteschi, D., Kahn, O., Miller, J. S., Palacio, F., Eds.; NATO ASI Series E 198; Kluwer: Dordrecht, The Netherlands, 1991.
(3) Caneschi, A.; Gatteschi, D.; Sessoli, R.; Rey, P. *Acc. Chem. Res.* **1989**, *22*, 392.
(4) Caneschi, A.; Ghatteschi, D.; Rey, P. *Prog. Inorg. Chem.* **1991**, *39*, 331.
(5) Johnson, S. A.; Hunt, H. R.; Neuman, H. M. *Inorg. Chem.* **1963**, *2*, 960.
(6) Lindsay, A. J.; Wilkinson, G.; Motevalli, M.; Hursthouse, M. B. *J. Chem. Soc., Dalton Trans.* **1987**, 2723.
(7) Cotton, F. A.; Norman, J. G., Jr. *J. Coord. Chem.* **1971**, *1*, 161.
(8) Richman, R. M.; Kuechler, T. C.; Tanner, S. P.; Drago, R. S. *J. Am. Chem. Soc.* **1977**, *99*, 1055.
(9) Bilgrien, C.; Drago, R. S.; Stahlbush, J. R.; Kuechler, T. C.; *Inorg. Chem.* **1985**, *24*, 4268.
(10) Cotton, F. A.; Felthouse, T. R. *Inorg. Chem.* **1982**, *21*, 2667.
(11) Felthouse, T. R.; Dong, T.-Y.; Hendrickson, D. N.; Shieh, H.-S.; Thompson, M. R. *J. Am. Chem. Soc.* **1986**, *108*, 8201.
(12) Cogne, A.; Grand, A.; Rey, P.; Subra, R. *J. Am. Chem. Soc.* **1989**, *111*, 3230.
(13) Norman, J. G., Jr.; Kolari, H. *J. Am. Chem. Soc.* **1978**, *100*, 791.
(14) Cotton, F. A.; Miskowski, V. M.; Zhong, B. *J. Am. Chem. Soc.* **1989**, *111*, 6177.

0020-1669/94/1333-3364$04.50/0

Table 1. Crystal Data and Experimental Parameters

formula	$C_{26}H_{36}F_{12}N_2O_{10}Ru_2$	
fw	960.65	
space group	$P\bar{1}$	
T, K	201	293
a, Å	8.748(2)	8.779(2)
b, Å	10.637(3)	10.728(3)
c, Å	11.495(3)	11.597(3)
α, deg	106.4(1)	107.1(1)
β, deg	103.2(1)	103.3(1)
γ, deg	107.7(1)	107.2(1)
V, Å^3	917.9	935.3
Z	2	2
ρ_{calcd}, g cm^{-3}	1.74	1.70
μ, cm^{-1}	9.3	9.0
R^a	0.057	0.038
$R_w{}^b$	0.057	0.040

^{a} $\Sigma||F_o| - |F_c||/\Sigma|F_o|$. ^{b} $(\Sigma w(|F_o| - |F_c|)^2/\Sigma w|F_o|^2)^{1/2}$; $w = 1/\sigma^2$.

Table 2. Atomic Positional Parameters (×10^4) for 1 at 293 K

	x	y	z	B_{EQ},^{a} Å^2
Ru	55(1)	912(1)	4665(1)	3.45
O1	1990(5)	2325(4)	6361(3)	4.55
O2	1772(5)	475(4)	3813(4)	4.44
O3	−1895(5)	−553(4)	2969(3)	4.50
O4	−1641(5)	1314(4)	5540(4)	4.52
O5	101(5)	2538(4)	3913(4)	5.16
N	−81(6)	3072(5)	3078(4)	4.26
F1	4805(7)	3941(6)	8394(5)	12.01
F2	3022(7)	3392(7)	9193(4)	11.37
F3	4647(7)	2342(6)	9023(5)	12.70
F4	4267(7)	−1432(6)	3679(5)	10.04
F5	4236(9)	131(7)	3018(8)	13.65
F6	2369(7)	−1892(8)	2025(5)	12.58
C1	2423(7)	1810(6)	7158(5)	4.16
C2	3743(9)	2879(7)	8461(6)	5.75
C3	2143(7)	−537(6)	3890(5)	4.12
C4	3271(9)	−919(8)	3146(7)	5.90
C5	−1856(10)	3091(9)	2614(8)	7.71
C6	−1677(12)	4292(10)	2125(10)	9.59
C7	−670(16)	4228(12)	1223(9)	10.41
C8	1083(14)	4506(13)	1932(13)	11.62
C9	1138(12)	3277(10)	2405(9)	8.05
C10	2890(10)	3720(9)	3350(9)	8.31
C11	475(19)	1747(12)	1248(10)	13.80
C12	−2401(12)	3487(12)	3853(10)	10.60
C13	−3075(10)	1705(8)	1674(8)	8.60

^{a} Defined as $(4/3)a^2B(1,1) + b^2B(2,2) + c^2B(3,3) + ab(\cos\gamma)B(1,2) + ac(\cos\beta)B(1,3) + bc(\cos\alpha)B(2,3)$.

$C_{46}H_{36}F_{20}N_2O_{10}Ru_2$: C, 40.64; H, 2.67; F, 27.97; N, 2.06; O, 11.78; Ru, 14.88. Found: C, 40.53; H, 2.56; F, 28.23; N, 2.15; Ru, 14.96. In the case of **1**, crystals suitable for a X-ray diffraction study were obtained by keeping the filtrate for 3 days at 4 °C. These crystals were also used for the magnetic measurements.

Magnetic Susceptibility Measurements. Magnetic data were obtained in the 2–300 K range by use of a Quantum Design MPMS superconducting SQUID susceptometer working at a 0.5-T field strength. The crude data were corrected for the contribution of the sample holder and the magnetic susceptibilities were corrected for the diamagnetism of the constituant atoms by use of Pascal constants.

X-ray Data Collection and Structure Determination. Preliminary Weissenberg photographs showed the triclinic system. A crystal of approximate dimensions 0.3 × 0.08 × 0.08 mm^3 was mounted on an Enraf-Nonius CAD-4 four-circle diffractometer equipped with graphite-monochromatized Mo Kα radiation and a low-temperature accessory. At both temperatures (293 and 201 K), the unit cell parameters were obtained from a least-squares fit of the automatically centered settings of 25 reflections; they are reported in Table 1 with other experimental parameters. Intensity data were corrected for Lorentz and polarization effects but not for absorption.

Space group $P\bar{1}$ was assumed and this initial choice was fully confirmed by all subsequent developments during the structure determination. The room temperature structure was solved by standard heavy-atom methods included in the SHELX86[15] package of structure determination. Difference Fourier maps revealed electron density contributions appropriately located for all non-hydrogen atoms. These were refined anisotropically; in the last refinement model, hydrogen atoms were included in fixed and calculated positions with isotropic thermal parameters equal to those of the connected carbon atoms. Owing to the similarity of the cell parameters at both temperatures, the positions of the atoms determined at 293 K were used as a starting refinement model for the low temperature structure. This procedure resulted in acceptable agreement factors which are reported in Table 1. Atomic positional parameters are found in Tables 2 and 3; selected bond lengths and angles are listed in Table 4.

A summary of crystal data and experimental parameters (Table SI), a complete listing of bond lengths (Tables SII and SIII) and angles (Tables SIV and SV), and listings of anisotropic thermal parameters (Tables SVI and SVII) are deposited as supplementary material.

Table 3. Atomic Positional Parameters (×10^4) for 1 at 201 K

	x	y	z	$B_{EQ}{}^a$
Ru	41(1)	932(1)	4672(1)	2.12
O1	1984(6)	2350(4)	6382(4)	3.01
O2	1774(6)	538(5)	3818(4)	2.83
O3	−1917(6)	−539(4)	2964(4)	2.88
O4	−1682(6)	1272(5)	5544(4)	3.07
O5	90(6)	2561(4)	3923(4)	2.97
N	−40(8)	3125(5)	3091(5)	2.92
C1	2444(8)	1828(7)	7178(6)	2.77
C2	3775(10)	2891(8)	8493(7)	3.68
C3	2183(8)	−449(7)	3905(6)	2.81
C4	3348(11)	−789(9)	3162(8)	4.15
C5	−1908(13)	3139(11)	2641(10)	6.01
C6	−1750(14)	4360(12)	2148(12)	7.12
C7	−837(15)	4127(16)	1185(11)	9.55
C8	1052(13)	4583(13)	1805(12)	7.36
C9	1049(18)	3299(13)	2340(12)	7.73
C10	2988(11)	3786(9)	3341(9)	4.88
C11	336(21)	1756(13)	1189(10)	10.45
C12	−2419(14)	3509(14)	3884(12)	8.09
C13	−3049(12)	1768(8)	1706(9)	5.06
F1	4863(8)	3960(6)	8400(5)	8.35
F2	3019(7)	3346(7)	9245(5)	7.73
F3	4705(8)	2328(6)	9046(5)	8.39
F4	4363(7)	−1309(7)	3692(5)	6.39
F5	4385(9)	350(8)	3096(8)	9.73
F6	2439(8)	−1710(8)	1980(5)	9.20

^{a} Defined as $(4/3)a^2B(1,1) + b^2B(2,2) + c^2B(3,3) + ab(\cos\gamma)B(1,2) + ac(\cos\beta)B(1,3) + bc(\cos\alpha)B(2,3)$.

Table 4. Selected Bond Lengths (Å) and Angles (deg) in 1

	T = 201 K	T = 293 K
Ru–Ru′	2.300(2)	2.293(1)
Ru–O1	2.066(3)	2.059(2)
Ru–O2	2.066(5)	2.073(5)
Ru–O3	2.083(3)	2.077(2)
Ru–O4	2.056(5)	2.062(5)
Ru–O5	2.136(5)	2.162(4)
O5–N	1.267(8)	1.265(7)
Ru′–Ru–O1	90.6(1)	90.6(1)
Ru′–Ru–O2	88.2(2)	88.6(1)
Ru′–Ru–O3	87.9(1)	88.0(1)
Ru′–Ru–O4	89.9(2)	89.9(1)
Ru′–Ru–O5	175.8(1)	176.5(1)
Ru–O5–N	158.2(3)	157.9(3)

Results

Structural Studies. As shown in Figure 1, $Ru_2(tfac)_4(Tempo)_2$ is a centrosymmetric bis(nitroxide) adduct, the center of symmetry being located at the midpoint of the Ru–Ru bond. The central $Ru_2(O_2C_2)_4$ core displays almost perfect D_{4h} symmetry and an eclipsed conformation identical to that observed in $Ru_2(tfac)_4(THF)_2$[6] as gauged by the dihedral angle O1–Ru–Ru′–O2′ (0.39 and 0.31°, respectively). Each Ru atom is in a tetragonally elongated environment, one of the axial positions being occupied

(15) Sheldrick, G. M. *Crystallographic Computing 3*; Sheldrick, G. M.; Kruger, C.; Goddard, R. Eds.; Oxford University Press: London, 1985, p 175.

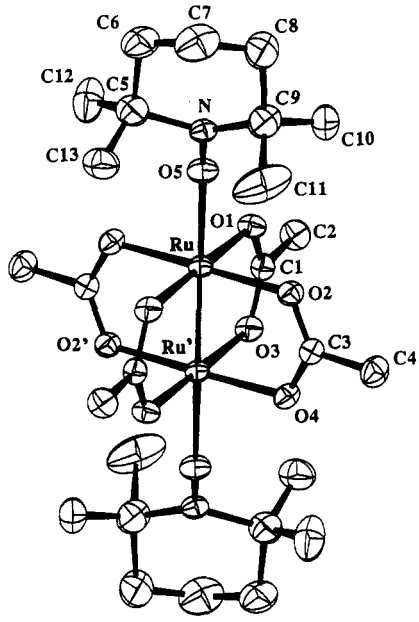

Figure 1. View of $Ru_2(tfac)_4Tempo_2$ as determined in the 293 K experiment. Thermal ellipsoids are drawn at the 30% probability level.

by a nitroxyl oxygen atom. The Ru–Ru distance is 2.293(1) Å at room temperature and 2.300(2) Å at 201 K, slightly longer than that observed in the precursor $Ru_2(tfac)_4(THF)_2$ (2.276(3) Å) and other paramagnetic ruthenium carboxylates where the Ru–Ru distance is shorter by *ca* 0.015 Å. These features are consistent with the strong electron-withdrawing properties of the CF_3 groups; they are also consistent with the presence of a double bond and exclude reduction of the dimetal core as observed for the adduct of $Ru_2(tfac)_4$ with NO.[6] In the trans position to the Ru–Ru bond are nitroxyl oxygen atoms at 2.162(4) and 2.136(5) Å at room and low temperatures, respectively. This shortening of 0.026(9) Å of the nitroxide binding distance at 201 K is the only significant difference observed in the two structural determinations. At both temperatures the axial nitroxyl oxygen atoms are nearly colinear with the Ru–Ru bond (Ru'–Ru–O5 = 176.5(1) and 175.8(1°), and their distance from each Ru atom is in accord with other oxygen-bonded adducts of $Ru_2(tfac)_4$. Each Ru atom is displaced by 0.025 Å out of the plane of four tfac oxygen atoms toward the nitroxide ligand. This ligand has the usual flattened chair conformation and pyramidal NO group (α = 14°) as observed in most uncoordinated piperidinyl nitroxides. The NO bond length of 1.267(2) Å affords further support to the free radical character of the ligand and the absence of redox process during the complexation. Since the Ru–O–N angle is 157°, this arrangement brings the four methyl groups of the ligand at similar distances from the metal basal plane (3.2–3.4 Å). In this respect, the binding of Tempo to $Ru_2(tfac)4$ is fairly different from that observed in the dirhodium derivative where the Rh–O–N angle is 138°.[11] All other structural features concerning the metal fragment and the radical ligand are unexceptional and need no further comments.

Magnetic Studies. According to the structural similarities of the diruthenium core in **1** and in the THF precursor, the same electronic structure and the same spin ground state will be assumed. Therefore, $Ru_2(tfac)_4(Tempo)_2$ will be considered as a three-spin system where the central S = 1 spin is exchange coupled with two $S = {}^1/_2$ nitroxide ligands. In the crystal, molecules related by cell translations are far apart so that intermolecular interactions will not be considered for interpreting the magnetic behavior of the complex.

The temperature dependence of the magnetic susceptibility data is shown in Figure 2 in the form of $\chi = f(T)$ and $\chi T = f(T)$ for $Ru_2(tfac)_2(Tempo)_2$. Worth to note is the sharp discontinuity observed at 243 K; below this temperature, both adducts **1** and

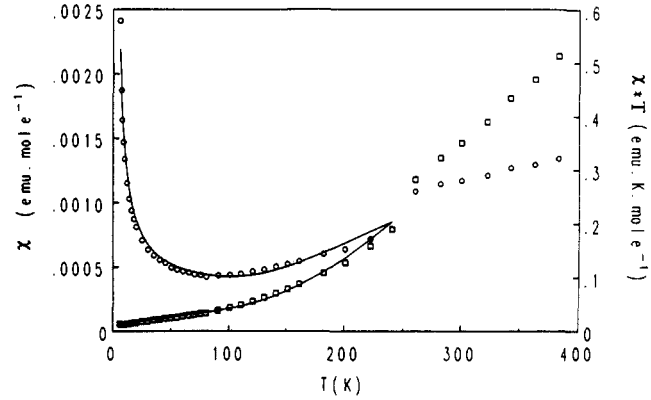

Figure 2. Temperature dependence of the magnetic susceptibility (○) and the product of the magnetic susceptibility with the temperature (□) for $Ru_2(tfac)_4Tempo_2$. The solid line was calculated with the parameters reported in Table 5.

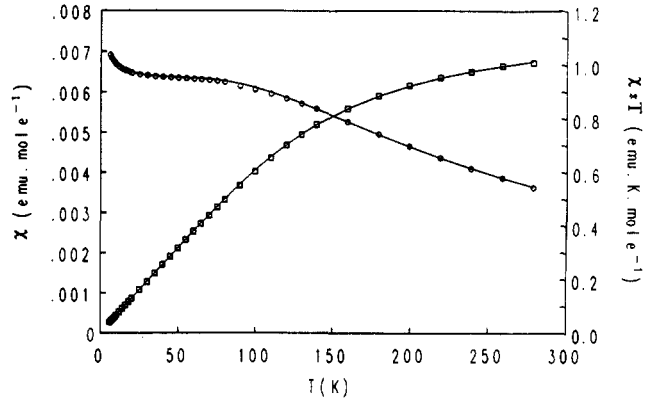

Figure 3. Temperature dependence of the magnetic susceptibility (○) and the product of the magnetic susceptibility with the temperature (□) for $Ru_2(tfac)_4THF_2$. The solid line was calculated with the parameters reported in Table 5.

2 exhibit the same behavior. For comparison, the same curves are diplayed in Figure 3 for $Ru_2(tfac)_2(THF)_2$. Qualitatively, one sees that the value of χT at 243 K is dramatically weaker (0.18 emu·K·mol^{-1}, 1.23 μ_B) in the nitroxide adducts than in the diruthenium precursor (0.98 emu·K·mol^{-1}, 2.8 μ_B) pointing to a strong antiferromagnetic interaction between the S = 1 dimetal core and the two paramagnetic ligands. Accordingly, a singlet ground spin state and a zero value of the susceptibility were expected at low temperature. The actual increase of the susceptibility data below 30 K is related to a small amount of uncoupled impurity (probably the oxidized Ru(II)–Ru(III) species) which must be taken into account for modeling the magnetic behavior of the compound.

Understanding of this behavior must also rely on the following considerations: (i) The magnetic properties of the diruthenium fragment are known to be dependent on a large zero-field splitting.[14] (ii) The single bond of the diamagnetic dirhodium moiety was reported to be an effective coupling pathway in $Rh_2(tfac)_4(Tempo)_2$[11] so that coupling of the two nitroxide ligands through the doubly-bonded diruthenium core must also be considered. Since these numerous contributions could have led to an overparametrized problem we examined first the magnetic properties of $Ru_2(tfac)_4(THF)_2$ in order to get a set of starting parameters describing the properties of the dimetal fragment.

$Ru_2(tfac)_4(THF)_2$ and $Ru_2(pfbz)_4(THF)_2$. As shown by Cotton,[14] the curve in Figure 3 is typical of a "spin-triplet, orbital-singlet ground state split in such a way that a nonmagnetic component lies lowest with the degenerate $S_z = \pm 1$ components being above by an amount comparable to kT". Assuming ideal D_{4h} symmetry, the π^{*2} configuration gives rise to the $^1A_{1g}$, $^1B_{1g}$, $^1B_{2g}$, and $^3A_{2g}$ states, split by a fairly large singlet-triplet separation

Table 5. Fitting Parameters for the Magnetic Data

	$Ru(tfac)_4$-$(THF)_2$	$Ru(pfbz)_4$-$(THF)_2$	**1**	**2**
g	2.0	2.0	2.0	2.0
D, cm^{-1}	235	243	235	243
TIP, 10^6 emu	308	448	256	168
P,[a] 10^2	0.4	0.6	1.1	0.8
J_2,[b] cm^{-1}			−263	−234
R,[c] 10^4	7.9	9.5	10.3	14.2

[a] P is an uncoupled impurity which as been modelized as the Ru(II)Ru(III) complex. [b] J_2 is the metal–nitroxide interaction. The Hamiltonian is defined as: $H = -2JS_iS_j$. [c] $R = \sum(X_{obsd} - X_{calcd})^2/\sum(X_{obsd})^2$.

$E_S = E_T = \delta$. The ground spin-triplet $^3A_{2g}$ is further split into a singlet level (A_{1g}) and a doubly degenerated (E_g) level by second-order effects of the spin-orbit coupling. Note that since a pseudo-vector transforms as $A_{2g} + E_g$,[16] the spin–orbit coupling connects only the $^3A_{2g}$ and $^1A_{1g}$ levels. Accordingly, the excited A_{1g} level also will be separated from the B_{1g} and B_{2g} by the same energy, D. Neglecting overlap of the Ru(II) orbitals and covalency effects of the ligands, calculations of the second-order effect of $\zeta(\vec{l}_1\vec{s}_1 + \vec{l}_2\vec{s}_2)$ lead to

$$D = \zeta^2/\delta$$

where ζ is the single-electron spin–orbit constant. Taking $\zeta \approx 1000\ cm^{-1}$,[17] and $\delta \approx 3000\ cm^{-1}$,[14] one obtains $D \approx 300\ cm^{-1}$. This value is probably overestimated because covalent effects are expected to weaken the value of ζ. However, this crude theory is in fairly good agreement with experimental values of $D \approx 250\ cm^{-1}$ reported so far for numerous examples.[14,18,19] Another result of these simple considerations concerns the effective gyromagnetic ratio, g_M, of the $^3A_{2g}$ triplet state. Any anisotropy would essentially arise from the cross term of the spin–orbit coupling and the Zeeman effect. Since between the excited singlet spin state $^1A_{1g}$ and the triplet ground state $^3A_{2g}$, there are no matrix elements of the total spin $s_1 + s_2$ and of the total angular momentum $l_1 + l_2$, the effective g factor is expected to be essentially isotropic and close to 2. For the same reasons, the temperature independent paramagnetism (Tip) should be comparable to that of a single ion with a $S = 1$ orbital-singlet ground state in a large crystal field. Typical expected values are in the (100–300) × 10^{-6} emu range.

With this guide line in mind, we fitted the experimental data of the two THF adducts to the theoretical expression of the magnetic susceptibility for an isotropic spin $S = 1$

$$\chi = (2Ng_M^2\mu_B^2/3kT)\{[e^{-x} + (2/x)(1 - e^{-x})]/(1 + 2e^{-x})\} + \text{Tip}$$

where $x = D/kT$ and the other parameters have their usual meaning. Since g_M and D are correlated, according to the preceding considerations g_M was set to 2.0. The best fit values are reported in Table 5. It should be noted that the agreement between experimental and calculated values is good and that values of the parameters are in close agreement with those expected from the above theory.

Switching to the bis-Tempo adducts, the expression of the magnetic susceptibility which takes into account a zero field splitting withing the dimetal fragment and coupling interactions between the three spins has been obtained as (see Appendix)

$$\chi = (N\mu_B^2/3k)F(T, g_M, g, J_1, J_2, D) + \text{Tip}$$

where F is a complicated expression derived in the Appendix, g_M and g are the g factors of the diruthenium core and the nitroxide ligands respectively, D is the zero-field splitting within the dimetal fragment, and J_1 and J_2 are the through-bond internitroxide coupling and the nitroxide–metal interaction respectively. Fitting the experimental data to this expression showed strong correlation between some parameters. Accordingly, g_M and D were fixed at values determined for the THF adduct; in addition the g value for the organic ligands was fixed at 2. It was noted that the quality of the fit was nearly independent of the value of J_1, which was set to zero. This result was expected since most of the three-spin systems reported so far exhibit the same property. The parameters which best-fit the data are listed in Table 5. Setting g_M to 2 and probable inaccurate estimation of the diamagnetism of the constituent atoms result in Tip values higher than expected. However, the values of J_2 are meaningful; they show that the metal–nitroxide interactions in **1** and **2** are antiferromagnetic and large.

Although the exact nature of the observed discontinuity in the magnetic behavior at 243 K in **1** is not known,[20] it is worth noting that a decrease of the Ru–O(nitroxyl) bond length at low temperature is qualitatively in agreement with a decrease of the magnetic susceptibility as observed in Figure 2.

Discussion

Binding of nitroxides to first row transition metals is well documented.[3,4,21,22] Schematically, bonding of Tempo or nitronyl nitroxides by the oyxgen atom occurs with a M–O–N angle close to 120° favoring orbital overlap and spin pairing. In contrast, N-bonded adducts of imino nitroxides exhibit a ferromagnetic behavior resulting from a coordination geometry of the imino nitrogen atom which brings magnetic orbitals orthogonal.[23,24] Exceptions to this rule include copper(II) complexes where a nitroxide ligand is axially coordinated. Although orthogonal magnetic orbitals are accounted for by this arrangement, it has been shown[25] that contribution from a delocalization mechanism could also explain the ferromagnetic behavior of these O-bonded adducts. However, simple geometric considerations allow to predict qualitatively the magnetic properties of metal–nitroxide complexes.

The same dichotomy has been observed in dirhodium–nitroxide magnetochemistry for O-bonded piperidinyl[11] or nitronyl nitroxide and N-bonded imino nitroxide species,[12] respectively. In the first type of complexes the through metal–metal bond coupling is strongly antiferromagnetic and since the coordination of the O(nitroxyl) atom occurs with a Rh–O–N angle close to 120°, it was suggested that the coupling pathway involved metal orbitals of σ symmetry. Further support to this suggestion came from the second type of complexes where the magnetic π^* orbital of the N-bonded nitroxide is parallel to the metal basal plane leading to weak positive or negative internitroxide interactions.[12]

Surprisingly, in $Ru_2(tfac)_4Tempo_2$, the binding geometry of the nitroxyl group closely resembles that observed in N-bonded dirhodium complexes or in axially O-bonded Cu(II) adducts; i.e., the Tempo magnetic orbital is almost parallel to the metal base plane. The magnetic behavior however, is strikingly different;

(16) Weisbluth, M. *Atoms and Molecules*; Academic Press: New York, 1978; Table 5.2.
(17) Abragam, A.; Bleaney, B. *Electron Paramagnetic Resonance of Transition Ions*; The Clarendon Press and Oxford University Press: London, 1969; Table 8.4.
(18) Cotton, F. A.; Ren, T.; Eglin, J. L. *J. Am. Chem. Soc.* **1990**, *112*, 3439.
(19) Maldivi, P.; Giroud-godquin, A.-M.; Marchon, J.-C.; Guillon, D.; Skoulios, A. *Chem. Phys. Lett.* **1989**, *157*, 552.
(20) Preliminary calorimetric measurements show that there is a phase transition which is not first order.
(21) Anderson, O. P.; Kuechler, T. C. *Inorg. Chem.* **1980**, *19*, 1417.
(22) Dickman, M. H.; Doedens, R. *J. Inorg. Chem.* **1981**, *20*, 2677.
(23) Luneau, D.; Rey, P.; Laugier, J.; Fries, P.; Caneschi, A.; Gatteschi, D.; Sessoli, R. *J. Am. Chem. Soc.* **1991**, *113*, 1245.
(24) Luneau, D.; Rey, P.; Laugier, J.; Belorizky, E.; Cogne, A.; *Inorg. Chem.* **1992**, *31*, 3578.
(25) Musin, R. N.; Schastnev, P. V.; Malinoskaya, S. A. *Inorg. Chem.* **1992**, *31*, 4118.

the dimetal fragment is now paramagnetic and a large antiferromagnetic interaction is observed showing that the π^* orbital of the NO groups does overlap with one (at least) of the metal-based magnetic orbitals. Among the orbital manifold of the diruthenium core only the π^* set has the right symmetry to overlap with the ligand magnetic orbital. Therefore, this study confirms the partial occupancy of the π^* metal orbitals in the ground state of the diruthenium tetracarboxylates.

Formation of adducts **1** and **2** proceeds without problem at room temperature and in the presence of oxygen. In contrast, attempts to prepare the homologous derivatives of nitronyl nitroxides led to instable compounds whatever the experimental conditions. Characterization of the hydroxylamine derived from the corresponding imino nitroxide is in line with previous reports. Conversion of a nitronyl nitroxide to the imino analogue and further reduction to the corresponding hydroxylamine have been observed in the presence of metal ions.[26-28]

Appendix

Susceptibility of the Bis-Tempo Adducts. The Hamiltonian of the system is

$$\mathcal{H} = \mathcal{H}_0 + \mu_B[g_M\vec{S} + g(\vec{s}_1 + \vec{s}_2)]\vec{H} \qquad (A1)$$

with

$$\mathcal{H}_0 = -2J_1\vec{s}_1\cdot\vec{s}_2 - 2J_2\vec{S}(\vec{s}_1 + \vec{s}_2) + D[S_z^2 - {}^1/_3\vec{S}^2] \qquad (A2)$$

where $s_1 = s_2 = {}^1/_2$ are the nitroxide spins and S = 1 is the spin of the diruthenium core. The meaning of J_1, J_2, D, g_M, and g are given in the text. The zero external field Hamiltonian $\mathcal{H}_0$ can be rewritten as

$$\mathcal{H}_0 = -J_1\vec{S}_{12}^2 - J_2(\vec{S}_t^2 - \vec{S}^2 - \vec{S}_{12}^2) + DS_z^2 + C \qquad (A3)$$

where C is a constant and where $\vec{S}_{12}$ and $\vec{S}_t$ are defined by

$$\vec{S}_{12} = \vec{s}_1 + \vec{s}_2 \qquad (A4)$$

$$\vec{S}_t = \vec{S}_{12} + \vec{S} \qquad (A5)$$

According to (A5), S_t is the total spin of the adduct. The Hamiltonian $\mathcal{H}_0$ is easily diagonalizable in the basis $|S,S_{12},S_t,M_t\rangle$. For $S_{12} = 1$, S_t can take the values 2, 1, 0, while for $S_{12} = 0$, $S_t = 1$. Altogether there are 12 states but only 8 energy levels. Below we list these levels with the associated eigenstates. Setting

$$\delta_1 = [4J_2^2 + D^2/4]^{1/2}$$

$$\delta_2 = [9J_2^2 + J_2D + D^2/4]^{1/2}$$

$$\cos\theta = [{}^1/_2(1 + 2J_2/\delta_1)]^{1/2}$$

$$\sin\theta = [{}^1/_2(1 - 2J_2/\delta_1)]^{1/2}$$

$$\cos\theta' = [1 + (3J_2 + D/6)/\delta_2)]/2^{1/2}$$

$$\sin\theta' = [1 - (3J_2 + D/6)/\delta_2)]/2^{1/2} \qquad (A6)$$

we obtain

eigenvalues of $\mathcal{H}_0 - C$	energy	eigenstates
E_1	$-2J_1 + J_2 + D/2 - \delta_2$	$\cos\theta'\|1120\rangle - \sin\theta'\|1100\rangle$
E_2	$-2J_1 + D/2 - \delta_1$	$\cos\theta\|1121\rangle - \sin\theta\|1111\rangle$ $-\cos\theta\|112{-}1\rangle - \sin\theta\|111{-}1\rangle$
E_3	$-2J_1 + 2J_2 + D$	$\|1110\rangle$
E_4	0	$\|1010\rangle$
E_5	D	$\|1011\rangle$ $\|101{-}1\rangle$
E_6	$-2J_1 + J_2 + D/2 + \delta_2$	$-\sin\theta'\|1120\rangle - \cos\theta'\|1100\rangle$
E_7	$-2J_1 + D/2 + \delta_1$	$-\sin\theta\|1121\rangle - \cos\theta\|1111\rangle$ $\sin\theta\|112{-}1\rangle - \cos\theta\|111{-}1\rangle$
E_8	$-2J_1 - 2J_2 + D$	$\|1122\rangle$ $\|112{-}2\rangle$

The susceptibility is then obtained from the Van Vleck theory, using the properties of trace invariance in a canonical transformation. The calculation is performed in the basis of the eigenstates of $\mathcal{H}_0$ and is given for N units in a polycrystalline sample by

$$\chi = \frac{N\mu_B^2}{3kT}\frac{1}{Z}\Big[\sum_i M_{ii}\exp(-E_i/kT) - 2kT\sum_{i\neq j} M_{ij}(\exp(-E_i/kT))/(E_i - E_j)\Big] \qquad (A7)$$

where

$$Z = \sum_i n_i\exp(-E_i/kT) \qquad (A8)$$

n_i being the multiplicity of the level E_i, where

$$M_{ii} = \sum_{k,k'} |\langle ik|\,\vec{\mathcal{M}}|ik'\rangle|^2 \qquad (A9)$$

$$M_{ij} = \sum_{k,l} |\langle ik|\,\vec{\mathcal{M}}|jl\rangle|^2 \qquad (A10)$$

with

$$\vec{\mathcal{M}} = g_M\vec{S} + g\vec{S}_{12} \qquad (A11)$$

In this notation the index k refers to the various eigenstates of $\mathcal{H}_0$ associated with the level E_i. From the above table we easily obtain the following: (a) diagonal matrix elements

$$M_{11} = M_{33} = M_{66} = 0$$

$$M_{22} = 2[{}^1/_2(g_M + g) + (g_M - g)\sin\theta\cos\theta]^2$$

$$M_{55} = 2g^2$$

$$M_{77} = 2[{}^1/_2(g_M + g) - (g_M - g)\sin\theta\cos\theta]^2$$

$$M_{88} = 2(g_M + g)^2 \qquad (A12)$$

(b) off-diagonal matrix elements ($M_{ij} = M_{ji}$)

$$M_{12} = 4\left[\sqrt{\frac{3}{8}}(g_M + g)\cos\theta\cos\theta' - \frac{1}{\sqrt{3}}(g_M - g)\left(\frac{1}{2\sqrt{2}}\sin\theta\cos\theta' + \sin\theta\sin\theta'\right)\right]^2$$

(26) Ullman, E. F.; Call, L.; Osiecki, J. H. *J. Org. Chem.* **1970**, *35*, 3623.
(27) Carducci, M. D.; Doedens, R. J. *Inorg. Chem.* **1989**, *28*, 2492.
(28) Caneschi, A.; Gatteschi, D.; Melandri, M. C.; Rey, P.; Sessoli, R. *Inorg. Chem.* **1990**, *29*, 4228.

$$M_{13} = {}^1/_3(g_M - g)^2 (\cos\theta' - \sqrt{2}\sin\theta')^2$$

$$M_{17} = 4\left[\sqrt{\frac{3}{8}}(g_M + g)\sin\theta\cos\theta' + \frac{1}{\sqrt{3}}(g_M - g)\left(\frac{1}{2\sqrt{2}}\cos\theta\cos\theta' + \cos\theta\sin\theta'\right)\right]^2$$

$$M_{23} = {}^1/_2[(g_M + g)\sin\theta + (g_M - g)\cos\theta]^2$$

$$M_{26} = 4\left[\sqrt{\frac{3}{8}}(g_M + g)\cos\theta\sin\theta' - \frac{1}{\sqrt{3}}(g_M - g)\left(\frac{1}{2\sqrt{2}}\sin\theta\sin\theta' - \sin\theta\cos\theta'\right)\right]^2$$

$$M_{27} = {}^1/_2(g_M - g)^2 (\cos^2\theta - \sin^2\theta)^2$$

$$M_{28} = [(g_M + g)\cos\theta + (g_M - g)\sin\theta]^2$$

$$M_{37} = {}^1/_2[(g_M + g)\cos\theta + (g_M - g)\sin\theta]^2$$

$$M_{45} = 2g^2$$

$$M_{67} = 4\left[\sqrt{\frac{3}{8}}(g_M + g)\sin\theta\sin\theta' + \frac{1}{\sqrt{3}}(g_M - g)\left(\frac{1}{2\sqrt{2}}\cos\theta\sin\theta' - \cos\theta\cos\theta'\right)\right]^2$$

$$M_{78} = [(g_M + g)\sin\theta - (g_M - g)\cos\theta]^2 \qquad \text{(A13)}$$

All other matrix elements are zero.

Note that the best fit of expression A7 with experimental data for compound 1, obtained with $J_1 = 0$, $J_2 = -250$ cm^{-1}, and $D = -250$ cm^{-1}, leads to a hierachy of the levels from E_1 to E_8 as indicated above. In particular we have a singlet ground state E_1 of $\mathcal{H}_0$ with a first excited doublet level E_2 with a splitting $E_2 - E_1 = -J_2 - \delta_1 + \delta_2 = 452.7$ cm^{-1}.

Supplementary Material Available: Summary of crystal data (Table SI) and listings of bond lengths (Table SII and SIII), bond angles (Tables SIV and SV), and anisotropic thermal parameters (Tables SVI and SVII) (9 pages). Ordering information is given on any masthead page.